catalysts

MDPI

Article

CO and CO_2 Co-Methanation on Ni/CeO_2-ZrO_2 Soft-Templated Catalysts

Luciano Atzori, Elisabetta Rombi, Daniela Meloni, Maria Franca Sini, Roberto Monaci and Maria Giorgia Cutrufello *

Dipartimento di Scienze Chimiche e Geologiche, Università di Cagliari, 09124 Cagliari, Italy; lucianoatzori@hotmail.it (L.A.); rombi@unica.it (E.R.); dmeloni@unica.it (D.M.); sini@unica.it (M.F.S.); monaci@unica.it (R.M.)

* Correspondence: gcutrufe@unica.it

Received: 30 March 2019; Accepted: 1 May 2019; Published: 2 May 2019

Abstract: Supported nickel catalysts were synthesized, characterized, and employed in the carbon oxides co-methanation process. Five NiO/CeO_2-ZrO_2 mixed oxides, with the same Ni content and different Ce/Zr molar ratios, were prepared by the soft-template method. They were characterized through ICP-AES, N_2 adsorption, XRD, and TPR. Reduced Ni/CeO_2-ZrO_2 catalysts were obtained by submitting the oxide systems to reduction treatment in H_2 at 400 °C. They were characterized by XRD, H_2-TPD, and CO_2 adsorption microcalorimetry and their catalytic performances in the carbon oxides co-methanation were investigated. Catalytic tests were performed in a fixed-bed continuous-flow microreactor at atmospheric pressure. The effect of experimental conditions (reaction temperature, space velocity, reactants molar ratio) was also studied. Almost complete CO conversion was obtained on any catalyst, whereas CO_2 conversion was much lower and increased with Ce content, at least up to Ce/Zr = 1. The beneficial effect of the Ce content could be related to the increased NiO reducibility and to the higher ability to adsorb and activate CO_2. However, at high Ce/Zr ratios, it is probably counterbalanced by an interplay of reactions involving CO and CO_2.

Keywords: carbon oxides; co-methanation; nickel-based catalysts; CeO_2-ZrO_2 supports; soft-template method

1. Introduction

Due to the depleting nature of oil and natural gas reserves, the production of a valuable fuel such as synthetic natural gas (SNG) has been attracting increasing attention. SNG can be obtained by hydrogenation of CO and/or CO_2 [1]. When syngas or hydrogen is obtained from renewable resources, carbon oxides methanation presents the additional advantage of reducing greenhouse gases emissions. Generally, reformed gases deriving from the steam reforming of oil fractions or from coal gasification contain both CO and CO_2. Thus, carbon oxides can be simultaneously hydrogenated to methane (co-methanation). Several studies have been devoted to the methanation of either CO [2–20] or CO_2 [5,21–42] on different supported metal catalysts. In some cases methanation of syngas containing both carbon oxides has been investigated with the aim of selectively hydrogenating CO [7,10,13,17–19]. However, a still limited number of papers deal with catalytic co-methanation of carbon oxides [43–52].

Supported nickel-based catalysts are generally very active and selective in carbon oxides hydrogenation reactions; the additional advantage of being reasonably inexpensive makes them promising alternatives to noble metals-based catalysts (e.g., supported Ru or Rh). As for the co-methanation process, several oxidic systems have been used as a support for nickel in combination with another metal [45,47,51,52]. For supporting undoped nickel, besides Al_2O_3 [47,51], CeO_2-Al_2O_3 [50], and Gd_2O_3-CeO_2 [52] systems, zirconia—pure [43,46] or in combination with other

oxides [43,46,48]—has been studied. When compared to pure zirconia, the presence of a second oxide has usually proved to be beneficial, especially for the thermal stability of the catalytic system [43,46]. On the other hand, when zirconia has been used in combination with ceria [48], only one composition has been studied, and no comparison with the pure oxides has been carried out. Recently, in the present authors' laboratory a series of undoped nickel catalysts, supported on pure and mixed cerium and zirconium oxides, has been synthesized and tested in the CO_2 hydrogenation to SNG, indicating the role of the CeO_2 component of the support in activating CO_2 [42].

In the present work a series of nanostructured NiO-CeO_2-ZrO_2 systems with different Ce/Zr ratios—including pure ZrO_2 and pure CeO_2—has been prepared by the unconventional soft-template synthetic method [53]. The mixed oxides have been characterized as for their structural, textural, and redox properties. The supported nickel catalysts have been obtained by in situ reduction of the synthesized systems. Their structure and their H_2 and CO_2 adsorption properties have also been studied and related to their catalytic performance in the carbon oxides co-methanation process, for which the effect of both the support composition and the reaction conditions (reaction temperature, space velocity, reactants molar ratio) was investigated.

2. Results

2.1. Characterization of Fresh NiO-CeO_2-ZrO_2 Mixed Oxides

NiO-CeO_2-ZrO_2 mixed oxides with a nominal NiO content of 30 wt% and different Ce/Zr molar ratios were synthesized by means of the soft-template method and will hereafter be referred to as NiO/$Ce_xZr_{1-x}O_2$, where x is the nominal CeO_2 molar fraction in the $(CeO_2)_x$-$(ZrO_2)_{1-x}$ support. Their chemical composition was determined by inductively coupled plasma atomic emission spectroscopy (ICP-AES). Data reported in Table 1 show that the experimental composition is close to the nominal one for all the samples.

Table 1. Chemical composition and textural features of the NiO/$Ce_xZr_{1-x}O_2$ samples.

Sample	NiO Content (wt%) [a]	CeO_2 Molar Fraction in $(CeO_2)_x$-$(ZrO_2)_{1-x}$ [a]	S_{BET} (m^2 g^{-1}) [b]	V_p (cm^3 g^{-1}) [b]
NiO/ZrO_2	30.2	-	282	0.27
NiO/$Ce_{0.25}Zr_{0.75}O_2$	29.5	0.263	245	0.23
NiO/$Ce_{0.50}Zr_{0.50}O_2$	29.0	0.507	245	0.31
NiO/$Ce_{0.75}Zr_{0.25}O_2$	29.1	0.737	198	0.28
NiO/CeO_2	29.0	-	197	0.31

[a] ICP-AES results. [b] From N_2 adsorption data.

Textural analysis was carried out by determining the nitrogen adsorption-desorption isotherms at −196 °C, which are shown in Figure 1. All the samples are characterized by a type IVa N_2 adsorption isotherm [54]; however, increasing Zr content results in a higher microporous contribution (at low p/p_0) and a more linear rise at high relative pressure ($p/p_0 > 0.6$). The pore size distribution curves, obtained by applying the BJH method to the isotherm adsorption branch [54,55], are displayed in the insets in Figure 1. They show a general decrease in pore size with increasing Zr content. In particular, at low Ce contents in the $(CeO_2)_x$-$(ZrO_2)_{1-x}$ support ($x \leq 0.25$) the contribution of pores wider than 10 nm becomes negligible. Specific surface area calculated using the BET equation (S_{BET}) and specific pore volume (V_p) are reported in Table 1. The pure zirconia-supported sample is characterized by a high surface area, which generally decreases with increasing Ce content.

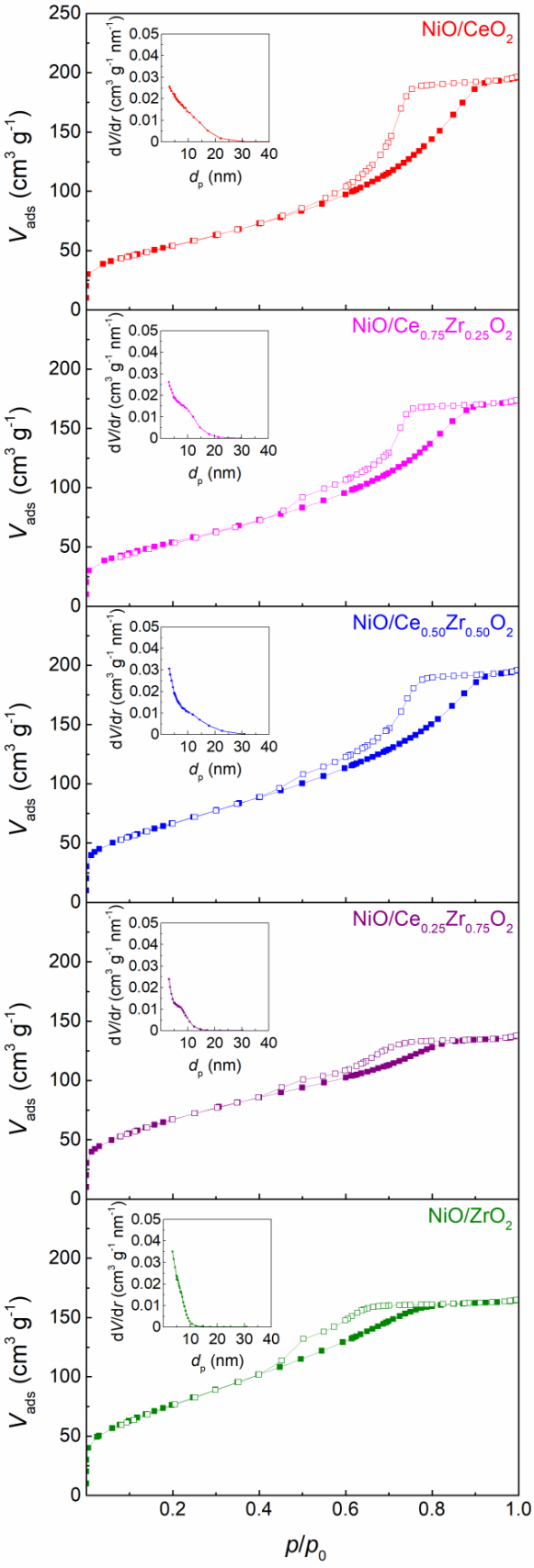

Figure 1. N_2 adsorption (full symbols) and desorption (open symbols) isotherms and pore size distribution curves (insets) of the NiO/$Ce_xZr_{1-x}O_2$ samples.

The X-ray diffraction (XRD) patterns of the fresh NiO-CeO_2-ZrO_2 systems are shown in Figure 2. In all samples, NiO crystalline phase (PDF Card 441159) can be identified, and from the peak width (by means of the Scherrer equation [56]) an average crystallite size of ca. 4 nm can be calculated. In the XRD patterns of NiO/ZrO_2 and NiO/CeO_2, signals ascribable to the corresponding pure oxide supports are also present. However, while the typical signals of nanocrystalline cubic CeO_2 phase (PDF Card 750151) can be identified, from which an average crystalline size of ca. 3 nm can be calculated, only one broad band ascribable to amorphous zirconia can be observed. In all the samples containing both Ce and Zr, besides the pure oxides (nanocrystalline ceria and amorphous zirconia), a ceria-zirconia solid solution is possibly present. In fact, signals corresponding to a cubic CeO_2-like phase are visible. With increasing Zr content, they become wider and shift towards higher angles, suggesting the (at least partial) incorporation of the small zirconium ions into the ceria lattice, which would lead to the formation of $Ce_xZr_{1-x}O_2$ solid solutions characterized by smaller crystallite size and lattice parameter.

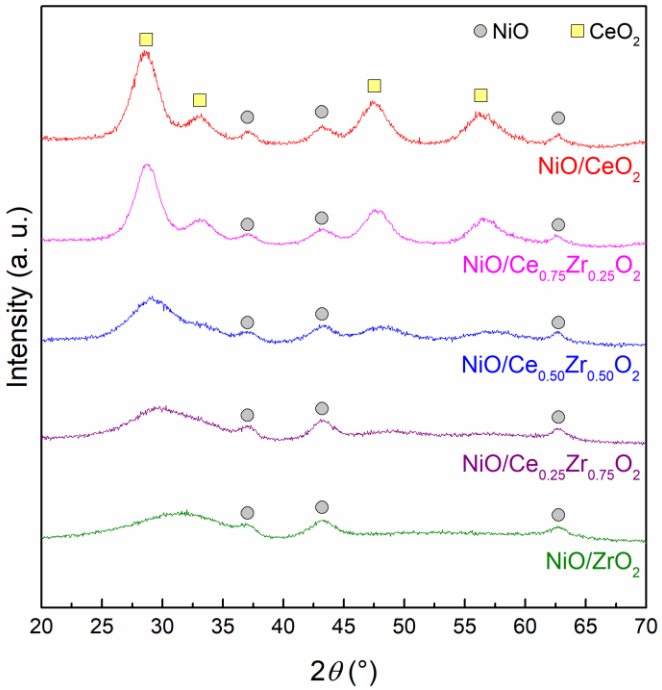

Figure 2. XRD patterns of the fresh NiO/$Ce_xZr_{1-x}O_2$ samples.

2.2. Reducibility of NiO-CeO_2-ZrO_2 Mixed Oxides And Characterization of the Reduced Samples

Reducibility of NiO-CeO_2-ZrO_2 mixed oxides was investigated by means of temperature-programmed reduction (TPR) analyses, whose results are reported in Figure 3. The TPR profile of NiO/ZrO_2 shows a single signal (maximum at ca. 590 °C) which—taking into account that soft-templated pure zirconia did not give rise to any significant hydrogen consumption [42]—can be ascribed to the reduction of the NiO species present in the sample. However, when compared with the position of the maximum (ca. 500 °C) in the TPR profile of a soft-templated pure NiO sample [42], such signal appears shifted to higher temperature, thus indicating the presence of strong ZrO_2-NiO interactions, which make the nickel oxide species more difficult to reduce. The TPR curves of the cerium-containing samples show a low-temperature (150–350 °C) small signal and a major one at higher temperatures. Both signals result from the overlapping of different contributions, which indicates the presence of different reducible species. Although also CeO_2 species can be reduced, most hydrogen consumption is expected to be due to the reduction of NiO species [42]. The features of the NiO/CeO_2 TPR profile can be described in the light of the literature on NiO-CeO_2 systems [19,42,57–59]. The low-temperature feature can be ascribed to the loss of oxygen species adsorbed on defective sites at the NiO-CeO_2 interface, where Ce

and Ni are in close interaction. The high-temperature signal clearly results from the partial overlapping of at least two contributions, which can be assigned to the reduction of nickel oxide particles dispersed on the ceria surface and to NiO species strongly interacting with CeO_2. Contributions similar to those distinguished for the pure ceria-supported sample are also present in the TPR curves of the systems containing both Ce and Zr, although with different relative areas.

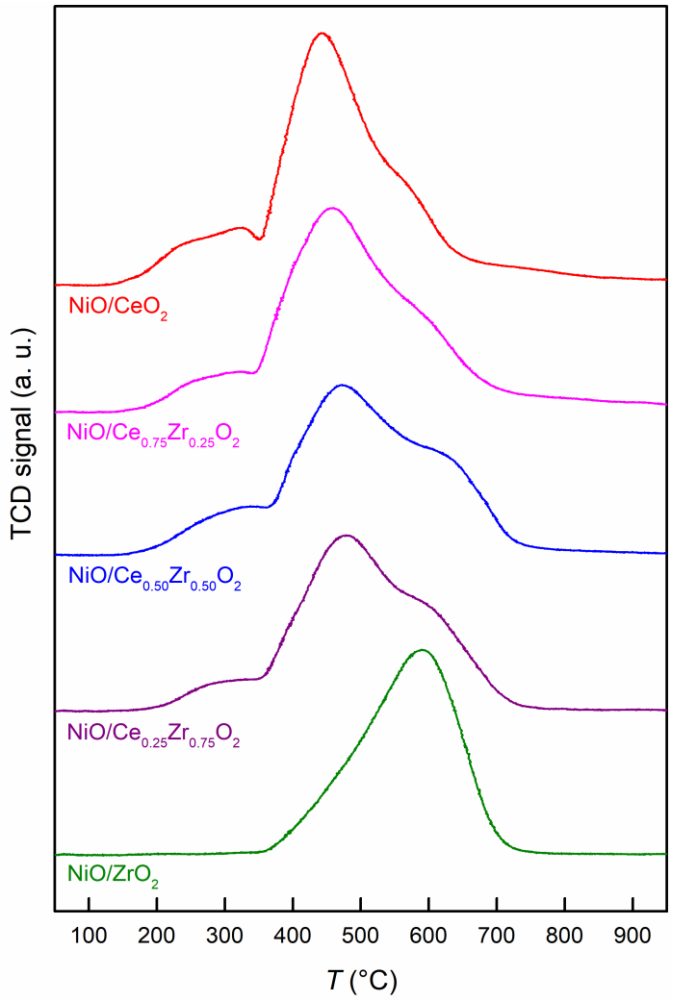

Figure 3. TPR curves of the NiO/$Ce_xZr_{1-x}O_2$ samples.

The synthetized systems were also characterized after being submitted to the same reduction pretreatment that they undergo prior to the catalytic tests (flowing H_2 at 400 °C for 1 h). The reduced samples will hereafter be referred to as Ni/$Ce_xZr_{1-x}O_2$. The XRD patterns of the hydrogen-treated systems are reported in Figure 4. As expected, the signals ascribable to the oxidic supports (amorphous zirconia, cubic ceria, and cubic solid solutions) are the same as those of the fresh NiO/$Ce_xZr_{1-x}O_2$ samples (cf. Figure 2). For all the reduced systems, signals of Ni^0 phase (PDF Card 040850) are present. The metallic nickel average crystal size, calculated by means of the Scherrer equation, is ca. 6 nm for all the Ce-containing samples, and lower than 5 nm for Ni/ZrO_2. Such small values indicate that the strong interaction with the support can hinder the sintering of the metal nanocrystals. The asymmetry of the main signals in the Ni/ZrO_2 pattern is probably due to some unreduced NiO, whose presence also in the other samples cannot be excluded.

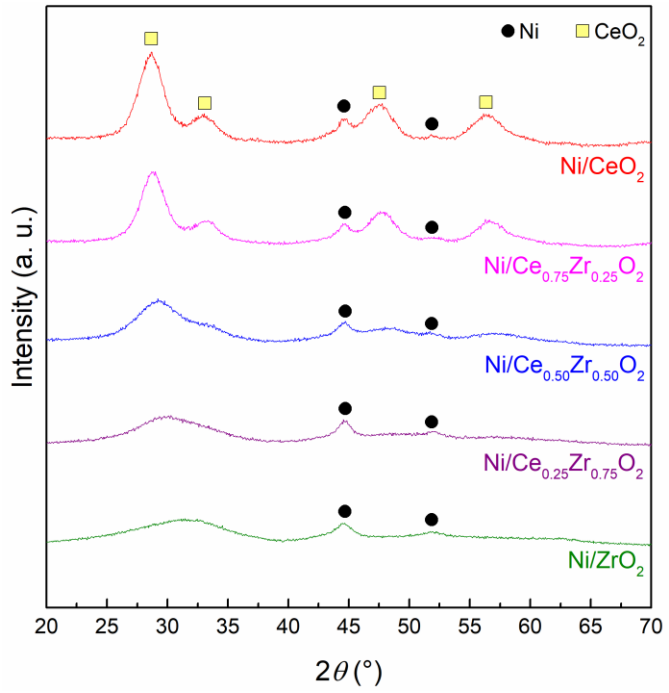

Figure 4. XRD patterns of the Ni/$Ce_xZr_{1-x}O_2$ samples.

The H_2 adsorption properties where studied through hydrogen temperature-programmed desorption (H_2-TPD) experiments. It resulted to be 55 μmol g^{-1} for Ni/ZrO_2 and to progressively increase with the Ce content up to 115 μmol g^{-1} for Ni/CeO_2. Probably the simple adsorption on the metallic Ni^0 surface is not the only cause for the total amount of hydrogen adsorbed, a contribution of spillover being expected. However, since the nickel content and the size of metal nanocrystals are similar for all the samples, the increasing trend of hydrogen adsorption with Ce content could mainly be explained by an increase in the NiO reduction degree at increasing Ce content. This would be in accordance with the TPR results and would imply that, even though no signals are clearly detectable in the XRD patterns, NiO phase is still present in the hydrogen-treated samples.

CO_2 adsorption properties of the Ni/$Ce_xZr_{1-x}O_2$ samples were studied through adsorption microcalorimetry. The differential heat of adsorption (Q_{diff}) is an indication of the strength of the adsorbent-adsorbate interaction, whereas CO_2 uptake is a measure of the number of adsorbing sites. Therefore, reporting Q_{diff} as a function of CO_2 uptake (Figure 5) simultaneous information on the concentration of the adsorbing sites and on their strength distribution is obtained. Whatever the sample, strong sites ($Q_{diff} \geq 150$ kJ mol^{-1}) are present in low concentration. As CO_2 uptake increases Q_{diff} decreases down to 50 kJ mol^{-1} (below which adsorption cannot be considered specific). For Ni/ZrO_2 such decrease is very steep and the total amount of CO_2 adsorbed is ca. 35 μmol g^{-1}. On the other hand, Ni/CeO_2 is able to adsorb a much higher amount of CO_2 (ca. 230 μmol g^{-1}), most of which on medium-strength sites (75 kJ $mol^{-1} \leq Q_{diff} \leq 150$ kJ mol^{-1}). These results, which are in agreement with those obtained on the pure oxidic phases [42], indicate the superior ability of CeO_2 – in comparison with ZrO_2 – in adsorbing and activating CO_2. The systems containing both Ce and Zr show an intermediate behavior, in terms of both concentration of adsorbing sites and strength of interaction. The general enhancement in the adsorption of CO_2 at increasing Ce content is not followed by Ni/$Ce_{0.50}Zr_{0.50}O_2$ and Ni/$Ce_{0.75}Zr_{0.25}O_2$, whose curves practically overlap. However, it has to be taken into account that the adsorption capacity also depends on the surface area, which for the reduced samples is expected to follow the same trend observed for the parent fresh oxide samples (Table 1). Compared to the sample with the same content of Ce and Zr, the Ce-richer sample is most probably characterized by a significantly lower surface area, which would counterbalance the higher capacity of the ceria component to adsorb CO_2.

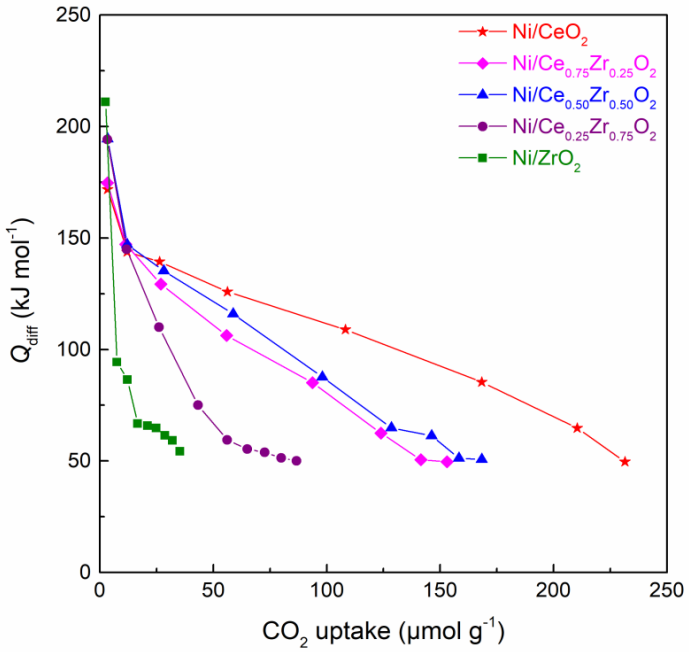

Figure 5. Differential heat of adsorption, Q_{diff}, as a function of CO_2 uptake on the $Ni/Ce_xZr_{1-x}O_2$ samples.

2.3. CO and CO_2 Co-Methanation Catalytic Tests

Simultaneous CO and CO_2 hydrogenation to SNG was carried out at 300 °C and atmospheric pressure on the $Ni/Ce_xZr_{1-x}O_2$ samples, obtained in the reduced form by in situ pretreatment (flowing H_2 at 400 °C for 1 h). A reactant gas mixture $CO/CO_2/H_2$ of molar composition of 1/1/5 was fed with a space velocity (SV) of 150,000 $cm^3\ h^{-1}\ g_{cat}{}^{-1}$. The results, in terms of CO and CO_2 conversions and methane selectivity, are summarized in Table 2. Since, during the 6-h runs, catalytic activity was found to be stable with time-on-stream (t.o.s) for all the samples, average values are reported.

Table 2. 6-h average CO conversion (X_{CO}), CO_2 conversion (X_{CO2}), and CH_4 selectivity (S_{CH4}) for the $Ni/Ce_xZr_{1-x}O_2$ samples in the CO_x co-methanation reaction. T = 300 °C; $CO/CO_2/H_2$ = 1/1/5; SV = 150,000 $cm^3\ h^{-1}\ g_{cat}{}^{-1}$.

Sample	X_{CO} (mol%)	X_{CO2} (mol%)	S_{CH4} (mol%)
NiO/ZrO_2	95	14	>99
$NiO/Ce_{0.25}Zr_{0.75}O_2$	95	16	>99
$NiO/Ce_{0.50}Zr_{0.50}O_2$	98	21	>99
$NiO/Ce_{0.75}Zr_{0.25}O_2$	98	21	>99
NiO/CeO_2	98	21	>99

Irrespective of the catalyst composition, a CH_4 selectivity higher than 99 mol% is always observed. All the catalysts exhibit very high CO conversion, which seems to be slightly favored by high Ce contents. CO_2 conversion is much lower and the beneficial effect of Ce is apparent up to an equimolar content of Ce and Zr, a further enrichment in Ce not producing any significant effect.

On $Ni/Ce_{0.50}Zr_{0.50}O_2$, a long-time run at variable temperature was carried out, to study the catalytic stability under thermal stress. As shown in Figure 6, both CO and CO_2 conversions decrease at increasing temperature, because of the exothermic character of both the CO and CO_2 methanation reactions. However, when the reaction temperature is set back at 300 °C, the catalytic activity is restored, indicating a very good thermal stability of the catalyst. Methane selectivity (not reported) was always higher than 99 mol%.

On $Ni/Ce_{0.50}Zr_{0.50}O_2$ the influence of both feed composition and space velocity was also investigated, by performing co-methanation at 300 °C with two different feed compositions ($CO/CO_2/H_2$ = 1/1/5

or 1/1/7) and three different space velocities (SV = 50,000, 150,000, or 450,000 $cm^3\ h^{-1}\ g_{cat}{}^{-1}$). Results reported in Figure 7 show that when a higher H_2 concentration is used CO_2 conversion significantly increases, whereas only a very slight improvement is observed for the already very high CO conversion. Whatever the feed composition, both X_{CO} and X_{CO2} decrease at increasing SV. However, whereas only small decreases in CO conversion are observed, the effect of SV on CO_2 conversion is particularly important, indicating that kinetic limitations are far more significant for CO_2 methanation. Noteworthy, for X_{CO2} the relative decrease is practically the same (ca. 37%) with either feed compositions. Also in these runs, methane selectivity (not reported) was always higher than 99 mol%.

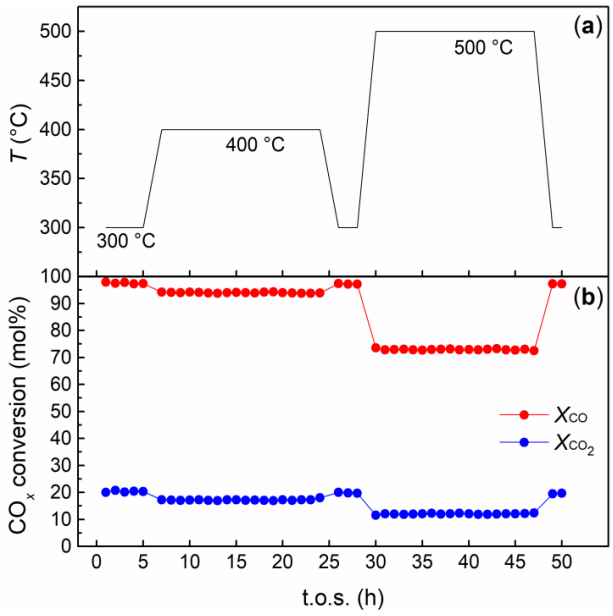

Figure 6. Thermal stability test for $Ni/Ce_{0.50}Zr_{0.50}O_2$ in the CO_x co-methanation reaction: (**a**) Reactor temperature profile; (**b**) CO conversion (X_{CO}) and CO_2 conversion (X_{CO2}) vs. time-on-stream (t.o.s.). $CO/CO_2/H_2$ = 1/1/5; SV = 150,000 $cm^3\ h^{-1}\ g_{cat}{}^{-1}$.

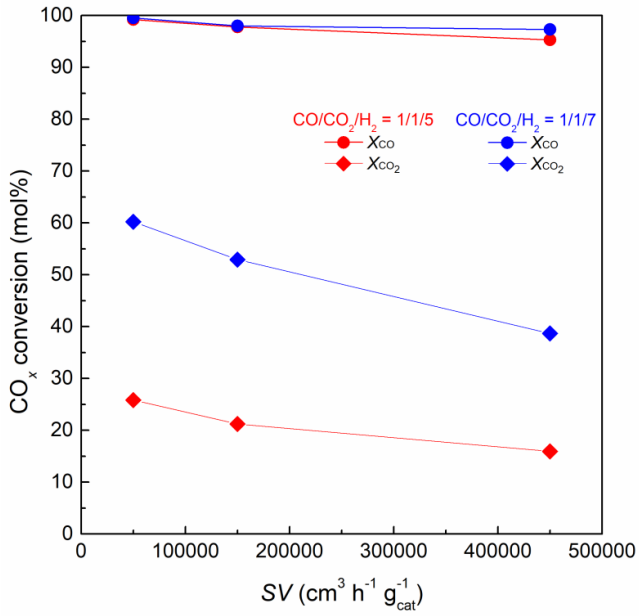

Figure 7. 6-h average CO conversion (X_{CO}) and CO_2 conversion (X_{CO2}) vs. space velocity (SV) for $Ni/Ce_{0.50}Zr_{0.50}O_2$ in the CO_x co-methanation reaction. T = 300 °C; red: $CO/CO_2/H_2$ = 1/1/5; blue: $CO/CO_2/H_2$ = 1/1/7.

3. Discussion

The NiO-CeO_2-ZrO_2 mixed oxides samples synthetized by the soft-template method are characterized by high surface areas and nanometric sizes of pores and crystallites. The strong interaction between the dispersed NiO phase and the ZrO_2 support makes the NiO nanoparticles reduction more difficult than for the unsupported nickel oxide. When Ce is present different reducible species are formed and reducibility generally increases. XRD results indicate the reduction of NiO nanocrystals under the experimental pretreatment conditions. However, H_2-TPD experiments suggest that such reduction is not complete, though favored by increasing Ce content.

In the carbon oxides co-methanation, a competition between CO and CO_2 hydrogenation reactions occurs. In the catalytic runs an almost complete CO conversion is obtained, whereas CO_2 is converted to a much smaller extent. The prevailing hydrogenation of CO rather than of CO_2 has already been reported [48,52] and is supported by thermodynamics [1]. Both reactions (Equations (1) and (2) in Scheme 1) are reversible and exothermic. Although both equilibrium constants decrease with temperature, at 300 °C still quite high values can be calculated, especially for CO hydrogenation [1].

$CO + 3\ H_2$	$\rightleftharpoons$	$CH_4 + H_2O$	ΔH = -206.1 kJ mol^{-1}	(1)
$CO_2 + 4\ H_2$	$\rightleftharpoons$	$CH_4 + 2\ H_2O$	ΔH = -165.0 kJ mol^{-1}	(2)
$2\ CO + 2\ H_2$	$\rightleftharpoons$	$CH_4 + CO_2$	ΔH = -247.3 kJ mol^{-1}	(3)
$CO + H_2O$	$\rightleftharpoons$	$CO_2 + H_2$	ΔH = -41.2 kJ mol^{-1}	(4)

Scheme 1. Stoichiometric equations for: (1) CO methanation; (2) CO_2 methanation; (3) reverse methane dry reforming; (4) water-gas shift [1].

On the present catalysts, CO hydrogenation is probably favored also from a kinetic point of view. In the co-methanation process, both the dispersed metallic nickel and the oxide support play a role. H_2 and CO are adsorbed and activated on metallic Ni^0 species [8]. On the other hand, adsorption and activation of CO_2 occur on the oxide support, through the intermediate formation of either CO or carbonate and hydrogencarbonate species [27]. Since CO is activated on the same sites as H_2, its hydrogenation is likely to be favored over that of CO_2, which requires the migration of adsorbed hydrogen from the metallic to the oxide phase (hydrogen spillover).

It has also to be taken into account that several other reactions might take place in the carbon oxides co-methanation system [1]. For the present catalytic tests, calculation of methane selectivity and carbon balance allow excluding the occurrence of reactions leading to C_{2+} hydrocarbons or to carbon deposits. However, CO and CO_2 are possibly involved also in reverse methane dry reforming and water-gas shift reactions (Equations (3) and (4) in Scheme 1). Although they are reversible reactions, CO conversion into CO_2 is thermodynamically favored; in particular, the reaction of reverse methane dry reforming is characterized by an equilibrium constant higher than those of the methanation reactions [1]. The combination of these reactions, or of the corresponding reverse reactions, with CO_2 or CO hydrogenation reactions would in the end lead to the production of methane. However, their occurrence needs to be considered when comparing the almost complete CO conversion and the low values obtained for CO_2 conversion. Most likely, not only CO_2 hydrogenation is repressed by the competitive CO hydrogenation, but CO_2 is also formed from CO. This is particularly true when the feed composition in the co-methanation runs is $CO/CO_2/H_2$ = 1/1/5, i.e., hydrogen concentration is lower than the stoichiometric amount. When hydrogen is fed in higher concentration ($CO/CO_2/H_2$ = 1/1/7; i.e., stoichiometric amount) CO_2 conversion significantly increases. However it does not reach the equilibrium value of 93 mol% [1], indicating the occurrence of kinetic limitations, as also suggested by the significant effect of *SV*.

The general beneficial effect of the Ce content on the catalytic activity of the present samples can be partly related to the increased reducibility of NiO species and the consequently higher amount of hydrogen adsorbed and activated. However, the role of the ceria component itself has to be taken

into account. Besides favoring CO activation on metallic Ni^0 [5,20], ceria is the main responsible for CO_2 adsorption and activation, as confirmed by the microcalorimetric results. CO_2 would preferentially adsorb on the ceria component of the support, most probably forming first carbonate and hydrogencarbonate species, which would then be hydrogenated to formates and finally to methane by the hydrogen previously adsorbed and activated by the metallic Ni^0 nanoparticles [27,36,38,42]. Therefore, the beneficial effect of the Ce content in the hydrogenation of CO_2 is most likely due also to the superior ability of CeO_2 in activating CO_2. However, a Ce molar fraction $x > 0.50$ in the support does not produce any further increase in X_{CO2}. In the light of the above description, this could be explained by the balance of different effects. As Ce content increases, increasing amounts of both CO_2 and H_2 can be adsorbed and activated. Therefore, increasing the Ce content up to Ce/Zr = 1 results in an increase in CO_2 conversion. A possible explanation for the observed behavior at Ce molar fraction $x > 0.50$ could be that the greater amount of activated hydrogen would favor the reverse methane dry reforming reaction. Thus, at high Ce contents the increased capacity in activating CO_2 would be counterbalanced by the increased amount of CO_2 produced through the reverse methane dry reforming reaction, resulting in a practically unchanged overall X_{CO2}. Further experiments should be performed in order to confirm such hypothesis.

Moreover, optimization of the co-methanation system, with the aim of obtaining higher CH_4 yields, could be achieved by analyzing the effect of the catalyst composition at different experimental conditions and better understanding the role of the catalytic active phases in the complex interplay of the different reactions involving carbon oxides.

4. Materials and Methods

4.1. Synthesis of Materials

$NiO\text{-}CeO_2\text{-}ZrO_2$ mixed oxides were synthesized by means of the soft-template method [53,60], using cetyl-trimethyl-ammonium bromide (CTAB, Aldrich, St. Louis, MI, USA, ≥ 98%) as templating agent, $Ni(NO_3)_2{\cdot}6H_2O$ (Aldrich, 99.999%), $Ce(NO_3)_3{\cdot}6H_2O$ (Aldrich, St. Louis, MI, USA, 99%), and $ZrO(NO_3)_2{\cdot}6H_2O$ (Aldrich, St. Louis, MI, USA, 99.999%) as precursors, and NaOH (Aldrich, St. Louis, MI, USA, 97%) as precipitating agent. For the synthesis, appropriate amounts of the template and the nitrate precursors (CTAB/precursors: 0.62 mol mol^{-1}; total precursors concentration: 0.048 M) were dissolved in distilled water at room temperature under stirring. After 30 min, a 0.15 M solution of NaOH was added dropwise until a pH value of 13 was reached; the mixture was then stirred for 15 h. After digestion at 90 °C for 3 h, the resulting solid was separated by filtration and washed with hot water (70 °C). It was then treated at 60 °C for 1.5 h, ground, dried at 110 °C for 6 h, and finally calcined at 450 °C for 4 h.

4.2. Characterization

Inductively coupled plasma atomic emission spectroscopy (ICP-AES) analyses were performed with a 5110 ICP-OES spectrophotometer (Agilent Technologies, Santa Clara, CA, USA) to determine the Ni, Ce, and Zr contents. Sample solutions were obtained by treating the solids with a H_2O_2 (35%) – HNO_3 (70%) mixture (1:1 by volume), stirring at 80 °C for 2 h, adding a HCl (37%) – HNO_3 (70%) mixture (3:1 by volume), and finally—after 16 h at RT—diluting with Milli-Q water.

Textural analysis was carried out with an ASAP 2020 system (Micromeritics), by determining the nitrogen adsorption-desorption isotherms at −196 °C. Before analysis, the sample was heated overnight under vacuum up to 250 °C (heating rate, 1 °C min^{-1}). Surface area values were calculated by the BET equation. The pore size distribution profiles were determined by applying the BJH method to the isotherm adsorption branch [55,56].

Structural characteristics of the fresh and reduced samples were investigated by X-ray diffraction (XRD) using a X3000 diffractometer (Seifert) with θ-θ Bragg-Brentano geometry with Cu-Kα wavelength

and a graphite monochromator before the detector. The average crystallite sizes were estimated by the Scherrer equation [56].

The studies on the reducibility of NiO-CeO_2-ZrO_2 mixed oxides and on the hydrogen adsorption properties of the reduced samples were performed by means of temperature-programmed reduction (TPR) and hydrogen temperature-programmed desorption (H_2-TPD) analyses, respectively, by using a TPD/R/O 1100 apparatus (ThermoQuest, Waltham, MA, USA) equipped with a thermal conductivity detector (TCD). Prior to the TPR experiment, the sample (typically 0.020 g) was pretreated in air (15 cm^3 min^{-1}) at 450 °C for 1 h; reduction profiles were then recorded under flowing H_2 (5 vol% in N_2; flow rate, 30 cm^3 min^{-1}) while heating (20 °C min^{-1}) from 40 to 950 °C. As for H_2-TPD analyses, the sample (ca. 0.100 g) was first reduced with pure H_2 (15 cm^3 min^{-1}) at 400 °C for 1 h. Then, after purge with N_2 at 400 °C for 1 h, pulses of H_2 (5 vol% in N_2) were admitted in the reactor at 50 °C until the area of the peaks was observed constant; finally, the desorption profile was collected under flowing N_2 (20 cm^3 min^{-1}) while heating (10 °C min^{-1}) from 40 to 500 °C.

CO_2 adsorption properties of the reduced samples were studied through adsorption microcalorimetry, using a Tian-Calvet heat flow calorimeter (Setaram, Caluire, France) connected to a volumetric vacuum line. Prior the analysis, each sample (ca. 0.150 g, 40 mesh) was reduced with pure H_2 at 400 °C for 1 h; then it was pretreated overnight at 250 °C under vacuum (10^{-3} Pa) before adsorption. CO_2 adsorption was carried out at 80 °C by admitting successive doses of the probe gas; for each dose, the equilibrium pressure, the amount of gas adsorbed, and the corresponding thermal effect were recorded. The run was stopped at the final pressure of 133.3 Pa.

4.3. CO and CO_2 Co-Methanation Catalytic Tests

Simultaneous CO and CO_2 hydrogenation to SNG was carried out in a tubular (i.d. = 0.8 cm) quartz-glass fixed-bed continuous-flow microreactor at atmospheric pressure. Prior to the reaction, the appropriate amount of catalyst powder was placed inside the reactor and pretreated in situ: It was first treated in flowing air (30 cm^3 min^{-1}) at 400 °C overnight; then, after purging in He (60 cm^3 min^{-1}), it was reduced under H_2 flow (15 cm^3 min^{-1}) at the same temperature for 1 h, and finally cooled to the reaction temperature in flowing He (60 cm^3 min^{-1}). The whole series of Ni/$Ce_xZr_{1-x}O_2$ catalysts was tested for 6 h at 300 °C, with a reactant gas mixture CO/CO_2/H_2 with molar composition of 1/1/5 (CO, 10 mol%; CO_2, 10 mol%; H_2, 50 mol%; balance N_2, used as internal standard) and space velocity (*SV*) 150,000 cm^3 h^{-1} $g_{cat}{}^{-1}$.

On Ni/$Ce_{0.50}Zr_{0.50}O_2$ additional runs were performed, also at different temperature (400 or 500 °C), with different CO/CO_2/H_2 molar composition (CO/CO_2/H_2 = 1/1/7: CO, 8 mol%; CO_2, 8 mol%; H_2, 56 mol%; balance N_2, used as internal standard), and/or at different space velocities (50,000 or 450,000 cm^3 h^{-1} $g_{cat}{}^{-1}$).

For each run, after the first hour on stream, on-line analysis of the reactor effluent was performed every hour (after removing water through an ice trap and a 3A molecular sieves trap, where no significant CO_2 adsorption proved to occur, placed between the reactor outlet and the injection valve) with a GC 6890 (Agilent), equipped with a HP Poraplot Q capillary column and a TCD. The results of the quantitative analysis of the carbon-containing components were used for checking the carbon mass balance and for calculating CO and CO_2 conversion and products selectivity.

5. Conclusions

NiO-CeO_2-ZrO_2 mixed oxides with narrow mesopores and high specific surface areas were prepared by the soft-template method. NiO was dispersed in the form of small crystallites on the CeO_2-ZrO_2 supports and its reducibility increased with the Ce content. Upon in situ reduction, active catalysts for the carbon oxides co-methanation were obtained. Whereas CO was almost completely converted, CO_2 conversion was much lower and resulted to depend on the catalyst composition. The increase in CO_2 conversion with Ce content up to Ce/Zr = 1 could be explained with the higher ability of the CeO_2 component of the support to adsorb and activate CO_2 and to promote NiO reduction,

thus also favoring H_2 adsorption and activation. However, at high Ce/Zr ratios, such effects are probably counterbalanced by the competition among the reactions involving H_2, CO, and CO_2.

Author Contributions: Conceptualization, L.A., E.R., and M.G.C.; Investigation, L.A., D.M., and M.F.S.; Resources, R.M.; Data curation, L.A.; Writing—Original draft preparation, M.G.C.; Writing—review and editing, L.A., E.R., and M.G.C.; Visualization, L.A. and M.G.C.; Supervision, E.R.; Project administration, E.R.

Funding: This research received no external funding.

Acknowledgments: The authors thank Fondazione di Sardegna (Progetti Biennali di Ateneo, Annualità 2017; CUP: F71I17000170002).

Conflicts of Interest: The authors declare no conflict of interest.

References

1. Gao, J.; Wang, Y.; Ping, Y.; Hu, D.; Xu, G.; Gu, F.; Su, F. A thermodynamic analysis of methanation reactions of carbon oxides for the production of synthetic natural gas. *RSC Adv.* **2012**, *2*, 2358–2368. [CrossRef]
2. Ishihara, T.; Eguchi, K.; Arai, H. Hydrogenation of Carbon Monoxide over SiO_2-Supported Fe-Co, Co-Ni and Ni-Fe Bimetallic Catalysts. *Appl. Catal.* **1987**, *30*, 225–238. [CrossRef]
3. Aksoylu, A.E.; Önsan, Z.İ. Interaction between Nickel and Molybdenum in Ni-Mo/Al_2O_3 catalysts: II. CO hydrogenation. *Appl. Catal. A Gen.* **1998**, *168*, 399–407. [CrossRef]
4. Xavier, K.O.; Sreekala, R.; Rashid, K.; Yusuff, K.; Sen, B. Doping effects of cerium oxide on Ni/Al_2O_3 catalysts for methanation. *Catal. Today* **1999**, *49*, 17–21. [CrossRef]
5. Znak, L.; Stołecki, K.; Zieliński, J. The effect of cerium; lanthanum and zirconium on nickel/alumina catalysts for the hydrogenation of carbon oxides. *Catal. Today* **2005**, *101*, 65–71. [CrossRef]
6. Kustov, A.L.; Frey, A.M.; Larsen, K.E.; Johannessen, T.; Nørskov, J.K.; Christensen, C.H. CO methanation over supported bimetallic Ni-Fe catalysts: From computational studies towards catalyst optimization. *Appl. Catal. A Gen.* **2007**, *320*, 98–104. [CrossRef]
7. Jimenez, V.; Sanchez, P.; Panagiotopoulou, P.; Valverde, J.L.; Romero, A. Methanation of CO, CO_2 and selective methanation of CO, in mixtures of CO and CO_2, over ruthenium carbon nanofibers catalysts. *Appl. Catal. A Gen.* **2010**, *390*, 35–44. [CrossRef]
8. Senanayake, S.D.; Evans, J.; Agnoli, S.; Barrio, L.; Chen, T.-L.; Hrbek, J.; Rodriguez, J.A. Water-Gas Shift and CO Methanation Reactions over Ni-CeO_2(111) Catalysts. *Top Catal.* **2011**, *54*, 34–41. [CrossRef]
9. Hu, D.; Gao, J.; Ping, Y.; Jia, L.; Gunawan, P.; Zhong, Z.; Xu, G.; Gu, F.; Su, F. Enhanced Investigation of CO Methanation over Ni/Al_2O_3 Catalysts for Synthetic Natural Gas Production. *Ind. Eng. Chem. Res.* **2012**, *51*, 4875–4886. [CrossRef]
10. Zhao, A.; Ying, W.; Zhang, H.; Ma, H.; Fang, D. Ni-Al_2O_3 catalysts prepared by solution combustion method for syngas methanation. *Catal. Commun.* **2012**, *17*, 34–38. [CrossRef]
11. Hwang, S.; Lee, J.; Hong, U.G.; Jung, J.C.; Koh, D.J.; Lim, H.; Byun, C.; Song, I.K. Hydrogenation of carbon monoxide to methane over mesoporous nickel-M-alumina (M = Fe, Ni, Co, Ce, and La) xerogel catalysts. *J. Ind. Eng. Chem.* **2012**, *18*, 243–248. [CrossRef]
12. Yan, X.; Liu, Y.; Zhao, B.; Wang, Z.; Wang, Y.; Liu, C.-J. Methanation over Ni/SiO_2: Effect of the catalyst preparation methodologies. *Int. J. Hydrogen Energy* **2013**, *38*, 2283–2291. [CrossRef]
13. Zyryanova, M.M.; Snytnikov, P.V.; Gulyaev, R.V.; Amosov, Y.I.; Boronin, A.I.; Sobyanin, V.A. Performance of Ni/CeO_2 catalysts for selective CO methanation in hydrogen-rich gas. *Chem. Eng. J.* **2014**, *238*, 189–197. [CrossRef]
14. Shinde, V.M.; Madras, G. CO Methanation Toward the Production of Synthetic Natural Gas over Highly Active Ni/TiO_2 Catalyst. *AIChE J.* **2014**, *60*, 1027–1035. [CrossRef]
15. Meng, F.; Li, Z.; Liu, J.; Cui, X.; Zheng, H. Effect of promoter Ce on the structure and catalytic performance of Ni/Al_2O_3 catalyst for CO methanation in slurry-bed reactor. *J. Nat. Gas Sci. Eng.* **2015**, *23*, 250–258. [CrossRef]
16. Zheng, Y.; Ma, H.; Zhang, H.; Ying, W.; Fang, D. Ni-Ce-Al composite oxide catalysts synthesized by solution combustion method: Enhanced catalytic activity for CO methanation. *Fuel* **2015**, *162*, 16–22. [CrossRef]

17. Konishcheva, M.V.; Potemkin, D.I.; Snytnikov, P.V.; Zyryanova, M.M.; Pakharukova, V.P.; Simonov, P.A.; Sobyanin, V.A. Selective CO methanation in H_2-rich stream over Ni-, Co- and Fe/CeO_2: Effect of metal and precursor nature. *Int. J. Hydrogen Energy* **2015**, *40*, 14058–14063. [CrossRef]
18. Nematollahi, B.; Rezaei, M.; Nemati Lay, E. Preparation of highly active and stable NiO-CeO_2 nanocatalysts for CO selective methanation. *Int. J. Hydrogen Energy* **2015**, *40*, 8539–8547. [CrossRef]
19. Nematollahi, B.; Rezaei, M.; Nemati Lay, E. Selective methanation of carbon monoxide in hydrogen rich stream over Ni/CeO_2 nanocatalysts. *J. Rare Earth* **2015**, *33*, 619–628. [CrossRef]
20. Rombi, E.; Cutrufello, M.G.; Atzori, L.; Monaci, R.; Ardu, A.; Gazzoli, D.; Deiana, P.; Ferino, I. CO methanation on Ni-Ce mixed oxides prepared by hard template method. *Appl. Catal. A Gen.* **2016**, *515*, 144–153. [CrossRef]
21. Yamasaki, M.; Habazaki, H.; Asami, K.; Izumiya, K.; Hashimoto, K. Effect of tetragonal ZrO_2 on the catalytic activity of Ni/ZrO_2 catalyst prepared from amorphous Ni-Zr alloys. *Catal. Commun.* **2006**, *7*, 24–28. [CrossRef]
22. Ocampo, F.; Louis, B.; Roger, A.-C. Methanation of carbon dioxide over nickel-based $Ce_{0.72}Zr_{0.28}O_2$ mixed oxide catalysts prepared by sol-gel method. *Appl. Catal. A Gen.* **2009**, *369*, 90–96. [CrossRef]
23. Ocampo, F.; Louis, B.; Kiwi-Minsker, L.; Roger, A.-C. Effect of Ce/Zr composition and noble metal promotion on nickel based $Ce_xZr_{1-x}O_2$ catalysts for carbon dioxide methanation. *Appl. Catal. A Gen.* **2011**, *392*, 36–44. [CrossRef]
24. Takano, H.; Izumiya, K.; Kumagai, N.; Hashimoto, K. The effect of heat treatment on the performance of the Ni/(Zr-Sm oxide) catalysts for carbon dioxide methanation. *Appl. Surf. Sci.* **2011**, *257*, 8171–8176. [CrossRef]
25. Tada, S.; Shimizu, T.; Kameyama, H.; Haneda, T.; Kikuchi, R. Ni/CeO_2 catalysts with high CO_2 methanation activity and high CH_4 selectivity at low temperatures. *Int. J. Hydrogen Energy* **2012**, *37*, 5527–5531. [CrossRef]
26. Cai, W.; Zhong, Q.; Zhao, Y. Fractional-hydrolysis-driven formation of non-uniform dopant concentration catalyst nanoparticles of Ni/$Ce_xZr_{1-x}O_2$ and its catalysis in methanation of CO_2. *Catal. Commun.* **2013**, *39*, 30–34. [CrossRef]
27. Ussa Aldana, P.A.; Ocampo, F.; Kobl, K.; Louis, B.; Thibault-Starzyk, F.; Daturi, M.; Bazin, P.; Thomas, S.; Roger, A.-C. Catalytic CO_2 valorization into CH_4 on Ni-based ceria-zirconia. Reaction mechanism by operando IR spectroscopy. *Catal. Today* **2013**, *215*, 201–207. [CrossRef]
28. Liu, J.; Li, C.; Wang, F.; He, S.; Chen, H.; Zhao, Y.; Wei, M.; Evans, D.G.; Duan, X. Enhanced low-temperature activity of CO_2 methanation over highly-dispersed Ni/TiO_2 catalyst. *Catal. Sci. Technol.* **2013**, *3*, 2627–2633. [CrossRef]
29. Pan, Q.; Peng, J.; Sun, T.; Gao, D.; Wang, S.; Wang, S.D. CO_2 methanation on Ni/$Ce_{0.5}Zr_{0.5}O_2$ catalysts for the production of synthetic natural gas. *Fuel Process. Technol.* **2014**, *123*, 166–171. [CrossRef]
30. Takano, H.; Shinomiya, H.; Izumiya, K.; Kumagai, N.; Habazaki, H.; Hashimoto, K. CO_2 methanation of Ni catalysts supported on tetragonal ZrO_2 doped with Ca^{2+} and Ni^{2+} ions. *Int. J. Hydrogen Energy* **2015**, *40*, 8347–8355. [CrossRef]
31. Aziz, M.A.A.; Jalil, A.A.; Triwahyono, S.; Ahmad, A. CO_2 methanation over heterogeneous catalysts: Recent progress and future prospects. *Green Chem.* **2015**, *17*, 2647–2663. [CrossRef]
32. Zhou, G.; Liu, H.; Cui, K.; Jia, A.; Hu, G.; Jiao, Z.; Liu, Y.; Zhang, X. Role of surface Ni and Ce species of Ni/CeO_2 catalyst in CO_2 methanation. *Appl. Surf. Sci.* **2016**, *383*, 248–252. [CrossRef]
33. Danaci, S.; Protasova, L.; Lefevere, J.; Bedel, L.; Guilet, R.; Marty, P. Efficient CO_2 methanation over Ni/Al_2O_3 coated structured catalysts. *Catal. Today* **2016**, *273*, 234–243. [CrossRef]
34. Frontera, P.; Macario, A.; Ferraro, M.; Antonucci, P.L. Supported Catalysts for CO_2 Methanation: A Review. *Catalysts* **2017**, *7*, 59. [CrossRef]
35. Nizio, M.; Albarazi, A.; Cavadias, S.; Amouroux, J.; Galvez, M.E.; Da Costa, P. Hybrid plasma-catalytic methanation of CO_2 at low temperature over ceria zirconia supported Ni catalysts. *Int. J. Hydrogen Energy* **2016**, *41*, 11584–11592. [CrossRef]
36. Atzori, L.; Cutrufello, M.G.; Meloni, D.; Monaci, R.; Cannas, C.; Gazzoli, D.; Sini, M.F.; Deiana, P.; Rombi, E. CO_2 methanation on hard-templated NiO-CeO_2 mixed oxides. *Int. J. Hydrogen Energy* **2017**, *42*, 20689–20702. [CrossRef]

37. Ashok, J.; Ang, M.L.; Kawi, S. Enhanced activity of CO_2 methanation over Ni/CeO_2-ZrO_2 catalysts: Influence of preparation methods. *Catal. Today* **2017**, *281*, 304–311. [CrossRef]
38. Atzori, L.; Cutrufello, M.G.; Meloni, D.; Cannas, C.; Gazzoli, D.; Monaci, R.; Sini, M.F.; Rombi, E. Highly active NiO-CeO_2 catalysts for synthetic natural gas production by CO_2 methanation. *Catal. Today* **2018**, *299*, 183–192. [CrossRef]
39. Ratchahat, S.; Sudoh, M.; Suzuki, Y.; Kawasaki, W.; Watanabe, R.; Fukuhara, C. Development of a powerful CO_2 methanation process using a structured Ni/CeO_2 catalyst. *J. CO2 Util.* **2018**, *24*, 210–219. [CrossRef]
40. Yu, Y.; Bian, Z.; Song, F.; Wang, J.; Zhong, Q.; Kawi, S. Influence of Calcination Temperature on Activity and Selectivity of Ni-CeO_2 and Ni-$Ce_{0.8}Zr_{0.2}O_2$ Catalysts for CO_2 Methanation. *Top. Catal.* **2018**, *61*, 1514–1527. [CrossRef]
41. Shang, X.; Deng, D.; Wang, X.; Xuan, W.; Zou, X.; Ding, W.; Lu, X. Enhanced low-temperature activity for CO_2 methanation over Ru doped the Ni/$Ce_xZr_{(1-x)}O_2$ catalysts prepared by one-pot hydrolysis method. *Int. J. Hydrogen Energy* **2018**, *43*, 7179–7189. [CrossRef]
42. Atzori, L.; Rombi, E.; Meloni, D.; Monaci, R.; Sini, M.F.; Cutrufello, M.G. Nanostructured Ni/CeO_2-ZrO_2 catalysts for CO_2 conversion into SNG. *J. Nanosci. Nanotechnol.* **2019**, *19*, 3269–3276. [CrossRef]
43. Habazaki, H.; Yamasaki, M.; Zhang, B.P.; Kawashima, A.; Kohno, S.; Takai, T.; Hashimoto, K. Co-methanation of carbon monoxide and carbon dioxide on supported nickel and cobalt catalysts prepared from amorphous alloys. *Appl. Catal. A Gen.* **1998**, *172*, 131–140. [CrossRef]
44. Gogate, M.R.; Davis, R.J. Comparative study of CO and CO_2 hydrogenation over supported Rh-Fe catalysts. *Catal. Commun.* **2010**, *11*, 901–906. [CrossRef]
45. Kang, S.-H.; Ryu, J.-H.; Kim, J.-H.; Seo, S.-J.; Yoo, J.-D.; Sai Prasad, P.S.; Lim, H.-J.; Byun, C.-D. Co-methanation of CO and CO_2 on the Ni_X-Fe_{1-X}/Al_2O_3 catalysts; effect of Fe contents. *Korean J. Chem. Eng.* **2011**, *28*, 2282–2286. [CrossRef]
46. Huang, Y.-H.; Wang, J.-J.; Liu, Z.-M.; Lin, G.-D.; Zhang, H.-B. Highly efficient Ni-ZrO_2 catalyst doped with Yb_2O_3 for co-methanation of CO and CO_2. *Appl. Catal. A Gen.* **2013**, *466*, 300–306. [CrossRef]
47. Razzaq, R.; Zhu, H.; Jiang, L.; Muhammad, U.; Li, C.; Zhang, S. Catalytic Methanation of CO and CO_2 in Coke Oven Gas over Ni-Co/ZrO_2-CeO_2. *Ind. Eng. Chem. Res.* **2013**, *52*, 2247–2256. [CrossRef]
48. Razzaq, R.; Li, C.; Amin, N.; Zhang, S.; Suzuki, K. Co-methanation of Carbon Oxides over Nickel-Based $Ce_xZr_{1-x}O_2$ Catalysts. *Energy Fuels* **2013**, *27*, 6955–6961. [CrossRef]
49. Razzaq, R.; Li, C.; Usman, M.; Suzuki, K.; Zhang, S. A highly active and stable Co_4N/γ-Al_2O_3 catalyst for CO and CO_2 methanation to produce synthetic natural gas (SNG). *Chem. Eng. J.* **2015**, *262*, 1090–1098. [CrossRef]
50. Li, Y.; Zhang, Q.; Chai, R.; Zhao, G.; Liu, Y.; Lu, Y. Structured Ni-CeO_2-Al_2O_3/Ni-Foam Catalyst with Enhanced Heat Transfer for Substitute Natural Gas Production by Syngas Methanation. *ChemCatChem* **2015**, *7*, 1427–1431. [CrossRef]
51. Zhao, K.; Li, Z.; Bian, L. CO_2 methanation and co-methanation of CO and CO_2 over Mn-promoted Ni/Al_2O_3 catalysts. *Front. Chem. Sci. Eng.* **2016**, *10*, 273–280. [CrossRef]
52. Frontera, P.; Macario, A.; Malara, A.; Modafferi, V.; Mascolo, M.C.; Candamano, S.; Crea, F.; Antonucci, P. CO_2 and CO hydrogenation over Ni-supported materials. *Funct. Mater. Lett.* **2018**, *11*, 1850061. [CrossRef]
53. Xie, Y.; Kocaefe, D.; Chen, C.; Kocaefe, Y. Review of Research on Template Methods in Preparation of Nanomaterials. *J. Nanomater.* **2016**, *2016*, 2302595. [CrossRef]
54. Rouquerol, F.; Rouquerol, J.; Sing, K.S.W.; Llewellyn, P.; Maurin, G. *Adsorption by Powders and Porous Solids, Principles, Methodology and Applications*, 2nd ed.; Elsevier: Amsterdam, The Netherlands, 2014.
55. Groen, J.C.; Peffer, L.A.A. Perez-Ramirez, Pore size determination in modified micro- and mesoporous materials. Pitfalls and limitations in gas adsorption data analysis. *J. Micropor. Mesopor. Mater.* **2003**, *60*, 1–17. [CrossRef]
56. Klug, H.P.; Alexander, L.E. *X-Ray Diffraction Procedures*; Wiley: New York, NY, USA, 1962.
57. Jalowiecki-Duhamel, L.; Ponchel, A.; Lamonier, C.; D'Huysser, A.; Barbaux, Y. Relationship between Structure of $CeNi_XO_Y$ Mixed Oxides and Catalytic Properties in Oxidative Dehydrogenation of Propane. *Langmuir* **2001**, *17*, 1511–1517. [CrossRef]
58. Wei, Y.; Wang, H.; Li, K.; Zhu, X.; Du, Y. Preparation and characterization of $Ce_{1-x}Ni_xO_2$ as oxygen carrier for selective oxidation methane to syngas in absence of gaseous oxygen. *J. Rare Earths* **2010**, *28*, 357–361. [CrossRef]

59. Sagar, T.V.; Sreelatha, N.; Hanmant, G.; Surendar, M.; Lingaiah, N.; Rama Rao, K.S.; Satyanarayana, C.V.V.; Reddy, I.A.K.; Sai Prasad, P.S. Influence of method of preparation on the activity of La-Ni-Ce mixed oxide catalysts for dry reforming of methane. *RSC Adv.* **2014**, *4*, 50226–50232. [CrossRef]
60. Wang, Y.; Ma, J.; Luo, M.; Fang, P.; He, M. Preparation of High-Surface Area Nano-CeO_2 by Template-Assisted Precipitation Method. *J. Rare Earths* **2007**, *25*, 58–62.